Characterization of metal fatigue by optical second harmonic generation

*Heike Arnolds**[1], Anthony Kakoulli[2], Komalben Shah[2] and Eann Patterson[2]*

[1]Department of Chemistry, [2]School of Engineering, University of Liverpool, Liverpool, UK

KEYWORDS

Fatigue, second harmonic generation, crack, plastic zone.

ABSTRACT

The optical second harmonic response of a pre-fatigued titanium specimen to picosecond 800 nm pulses has been investigated. Polarization-dependent measurements show that the zxx component of the nonlinear susceptibility tensor $\chi^{(2)}$ differs markedly when measured in a region of unfatigued polycrystalline titanium compared to the plastic deformation zone ahead of a crack tip and even changes sign within the plastic wake. This tensor component is sensitive to bulk currents and we attribute the observed changes to a changed density of states at the Fermi level, caused by the accumulation of dislocations. Second harmonic polarization analysis could thus be useful in non-invasive fatigue analysis.

INTRODUCTION

Fatigue is "the single largest cause of failure in metals" [1] and thus of inherent interest in aerospace and automotive industries. In metals, cyclic loading causes dislocations to accumulate in regions where there is a concentration of stress that causes small-scale yielding of the material. This tends to occur at geometric discontinuities and, or where flaws or defects are present in the material. During a cyclic load, plastic deformation occurs within these structures as dislocations slip and concentrate in locations of high stress, coalescing to form voids and eventually cracks. A crack tip further concentrates stress, creating an area of plasticity ahead of the propagating crack. The role of the zone of plasticity ahead of a fatigue crack in controlling the rate of crack growth has been recognized for some time [2]. The ability to monitor this area of plasticity would be of great use in characterizing fatigue crack growth.

The only techniques currently available to monitor the plastic zone ahead of a crack [3] are either forensic, such as etching techniques, recrystallization and shear lip size measurements, or require prior knowledge of yield strength and material strain history for strain evaluation such as digital image correlation and Moiré interferometry[4]. Recently, thermal images of the heat generated during the movement of dislocations have been monitored to provide an indication of the size and shape of the plastic zone [5]; however, this technique has low spatial resolution and no sensitivity to dislocation density. Dislocation density has been assessed using X-ray diffraction[6] and scanning electron microscopy[7] but the instrumentation required does not lend itself to in-situ engineering investigations. There are no measurement techniques easily available to the engineer which can sense the evolution of the plastic zone ahead of a propagating crack with high spatial resolution and in a variety of environments.

Optical second harmonic generation (SHG) is frequently used in the analysis of surfaces, since it is forbidden in bulk achiral material in the dipole approximation [8]. It has thus found its main applications in surface chemistry and biology, and has over the past two decades evolved to a widely-applied technique [9-14]. In materials science, SHG has found an important application in monitoring how epitaxial strain and defects affect magneto-electric and optical properties of materials [15-20]. For metals, a significant focus has been on nanostructured surfaces or particles [9, 21, 22], where the high polarizability of electrons in plasmonic materials creates large second harmonic responses which can be used for sensing or general photonics applications. In addition, metals possess an important bulk SHG response, due to magnetic dipole and electric quadrupole contributions[23].

The second harmonic response of metals is known to be closely related to the electronic density of states and degree of delocalization of the electrons involved[24-26]. Dislocations in metals such as titanium have been found to alter the electronic density of states [27, 28] and it should therefore be possible to relate dislocation density to the second harmonic response. In this work, we show for a pre-fatigued polycrystalline Titanium specimen that optical second harmonic generation can indeed sense dislocation density with high spatial resolution of 100 μm. Polycrystalline Titanium is an important material in the aerospace and automotive industries and has been the subject of previous investigations of crack tip plastic zones [4, 29].

EXPERIMENTAL

The second harmonic spectrometer is based on a design [30, 31], which allows unambiguous measurement of the second order susceptibility tensor, by a combination of halfwave plate and rotating quarter wave plate (QWP). The QWP introduces a known phase difference between

incident s- and p-polarisation components which removes the ambiguity inherent in a pure intensity measurement.

An amplified 10 Hz femtosecond Ti:Sapphire system (Spectra Physics) provides 120 fs long pulses centered at 800 nm. The pulses are stretched in time by an etalon to 2 ps to reduce peak intensity and avoid specimen damage. A half wave plate polarizer sets the initial polarization to one of p, s, p+s or p-s. A quarter wave plate polarizer then modulates this initial polarization. Second harmonic produced by the input optics is removed by a long pass filter before reflection off the specimen under 30° and the fundamental is removed by short pass filter after reflection. The second harmonic light is focused into a 0.3 m Czerny-Turner spectrograph (Acton SpectraPro 300i) and recorded on typically 20 pixel (ca 0.5 mm) high track on an ICCD (Andor Technology). The signal is binned across the track and gated in a 20 ns window around the laser pulse to reduce noise. The specimen is positioned by manual micrometer stages from Thorlabs. The incoming pulse power was 5 μJ with a focal spot diameter of about 100 μm.

We used a 25 mm × 24 mm commercially-pure Titanium compact tension specimen (ASTM E647), with 1 mm thickness. A fatigue crack was grown by cyclic loading in a uniaxial loading frame (Electropulse E3000, Instron) at 20 Hz with a 600 N mean load and 150 N amplitude. During fatigue loading, thermoelastic stress analysis (TSA) was performed with a Deltatherm system 1750 (Stress Photonics Inc., Madison WI) with staring array infra-red detector with 640 x 512 pixels and thermal sensitivity of 20 mK. The magnitude of the thermoelastic signal is proportional to the first stress invariant; while its phase is of opposite sign to the loading signal under adiabatic conditions. Such TSA phase data can be used to determine the plastic zone size and shape data[5] by applying a binary filter and identifying the plastic zone as those locations where the phase difference was non-zero as a consequence of heat generation by dislocation

formation and movement. The resultant plastic zone is shown in Figure 1 as an area of constant blue colour, just beyond the crack tip, superimposed on the unfiltered phase data for the remainder of the TSA field of view. The area of the plastic zone is 1.23 mm^2 (approximately 1×1.6 mm). The red area of positive phase indicates where heat is being generated by contact between the crack flanks during unloading in the cycle, and the dark blue zones in the top and bottom left corners are attachments to the test machine.

The pre-fatigued specimen was electropolished to remove any oxide layer and to gain high reflectivity, which prevents beam damage by amplified picosecond pulses.

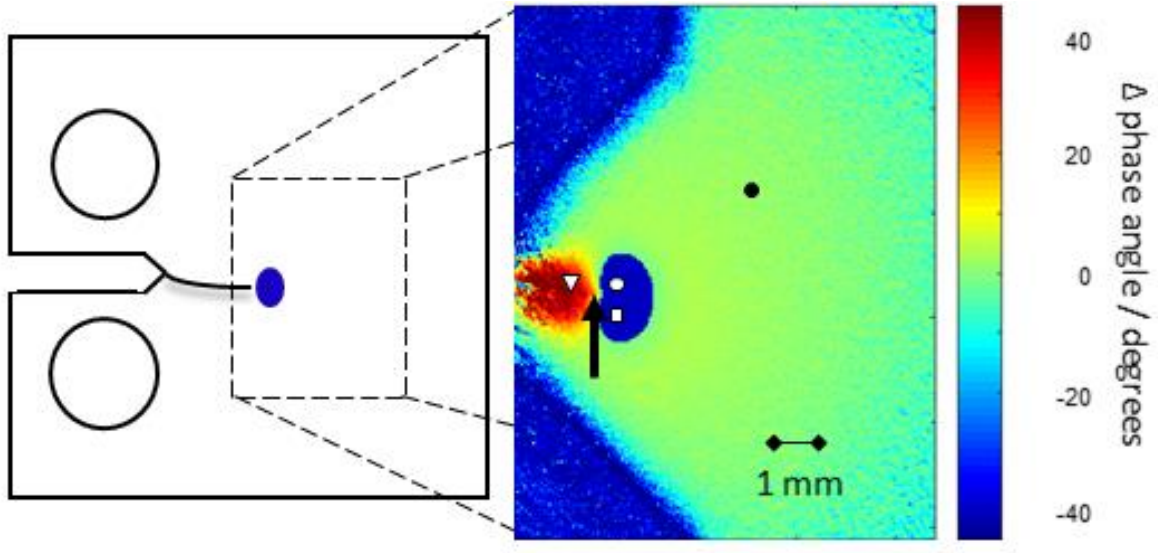

Figure 1: Left: Sketch of a tension specimen with propagating crack tip and schematic plastic zone. Right: Phase data obtained using thermoelastic stress analysis, after binary filter application. The color bar indicates the phase difference in degrees. The plastic zone has been assigned a dark blue colour, irrespective of individual pixel values to highlight its area. An image with the measured phase angles inside the plastic zone can be found in the supporting information. The arrow marks the crack tip. The symbols mark the spots which are polarization analyzed in Figure 2.

RESULTS

In second harmonic generation, an incident electric field at frequency ω generates a nonlinear polarization $P^{(2)}$ at frequency 2ω. In the electric dipole approximation, $P^{(2)}$ is given by:

$$P_i^{(2)}(2\omega) = \sum_{ijk} \chi_{ijk}^{(2)} E_j(\omega) E_k(\omega) \qquad (1)$$

where E(ω) is the incident field, $\chi^{(2)}$ is the second order susceptibility tensor and i,j,k are Cartesian coordinates. For symmetry reasons on a homogeneous achiral surface, only three distinct non-zero tensor components exist, namely $\chi^{(2)}_{zzz}$, $\chi^{(2)}_{zxx}$ and $\chi^{(2)}_{xxz} = \chi^{(2)}_{xzx}$. In a single beam measurement, with p-polarized incoming and outgoing beams, the signal contains contributions from all three tensor elements.

Strain, stress and dislocations can change the nonlinear polarizability $\chi^{(2)}$, though detailed studies have only been carried out for semiconducting or insulating materials. On silicon surfaces, for example, strain is generated at the interface between bulk and oxide layer due to lattice mismatch and $\chi^{(2)}$ varies with the ratio of interface strain to strain decay length[32].

On metal surfaces, the nonlinear polarizability is determined by the occupied and unoccupied electronic density of states near the Fermi level. Free electron metals such as gold, silver, copper and aluminum show the largest SH responses over a wide wavelength range [33, 34], in particular when transitions from the occupied d-band to the empty s-band are excited. For near-infrared excitation, several transition metals with localized d-electrons only showed a 30% lower than free electron metals [35], but not many direct comparisons have been made[36].

Within a free electron model of a metal with dielectric susceptibility $\varepsilon(\omega)$, Rudnick and Stern showed that the second order susceptibility tensor of a metal arises from three sources: currents which flow perpendicular and parallel to the surface and within the bulk [37]. P-polarized components of the bulk response are indistinguishable from the surface response in a single-beam experiment and the effective tensor components are given by [23]:

$$\begin{aligned} \chi^{(2)}_{zzz} &= \chi^{(2)}_{zzz,surf} + \frac{\gamma}{\varepsilon(2\omega)} \\ \chi^{(2)}_{zxx} &= \chi^{(2)}_{zxx,surf} + \frac{\gamma}{\varepsilon(2\omega)}, \\ \chi^{(2)}_{xxz} &= \chi^{(2)}_{xxz,surf} \end{aligned} \qquad (2)$$

where γ is the bulk contribution normalized by the dielectric function at the second harmonic frequency.

Surface nonlinearities generally overwhelm the bulk response in $\chi^{(2)}_{zzz}$, because they relate to the electron density gradient perpendicular to the surface and are thought to arise from the top 0.1 nm of the surface. A simple intensity measurement is therefore not very informative as demonstrated by several p-in, p-out SH linescans around the crack tip (shown in Figure S2 in the SI). This polarization combination is most sensitive to surface effects, while any dislocations arise much deeper in the bulk.The tensor component $\chi^{(2)}_{zxx}$ directly reflects the bulk contribution, because the surface component $\chi^{(2)}_{zxx,surf}=0$ in the hydrodynamic model frequently used to describe metal surfaces. $\chi^{(2)}_{zxx} = \gamma/\varepsilon(2\omega)$ is thus generated from lateral currents which arise from depths as large as several nm[38]. For d-band metals such as titanium, the effective probe depth is likely lower, due to the presence of localized d-electrons[26], but $\chi^{(2)}_{zxx}$ is still the tensor element which is most sensitive to bulk effects.

This relevant $\chi^{(2)}_{zxx}$ tensor component can be measured with a method which is largely independent of alignment [30, 31] and which provides unique values for the nonlinear susceptibility components for a single input beam. This method creates an incoming mixed polarization state, with a polarization vector halfway between p and s polarization, labelled as p+s or p-s polarization states. This mixed state is subsequently rotated by a quarter wave plate, which introduces a known phase modulation. We effectively measure:

$$I_p^{SHG} = \left| fE_p^2 + gE_s^2 \right|^2 \tag{3}$$

where the (generally complex-valued) coefficients are related to the second-order susceptibility components via $f \sim \chi^{(2)}_{tot} = a\chi^{(2)}_{zzz} + b\chi^{(2)}_{xxz} + c\chi^{(2)}_{zxx}$, and $g \sim \chi^{(2)}_{zxx}$ [30]. The size of the second harmonic signal does not depend on the absolute phase of the parameters f and g but on their relative phase. We can therefore choose f as real-valued and $g = g_1 + ig_2$. If a mixed polarization state is chosen, the QWP rotation results in an intensity variation of the SH intensity

$$I^{SHG} = a_0 + \sum_{m=1}^{4} \left[a_m \cos(2m\theta_{QWP}) + b_m \sin(2m\theta_{QWP}) \right]. \tag{4}$$

The Fourier components in equation (4) for the polarization states p±s then lead to unique values of f and $g_{1,2}$:

$$\begin{aligned} f &= \sqrt{\pm b_2 + 2\sqrt{b_2^2 + a_2^2 + 4a_3^2}} \\ g_1 &= -\frac{2a_1}{f} \\ g_2 &= \frac{4a_3}{f} \end{aligned} \tag{5}$$

We thus obtain both f, which represents the total susceptibility $\chi^{(2)}_{tot}$ for incoming and outgoing p-polarization, and g_1,g_2, the real and imaginary components of $\chi^{(2)}_{zxx}$. Even if $\chi^{(2)}_{tot}$ varies due to misalignment on uneven surfaces, a normalization relative to the total susceptibility provides a useful relative measure of the bulk contribution.

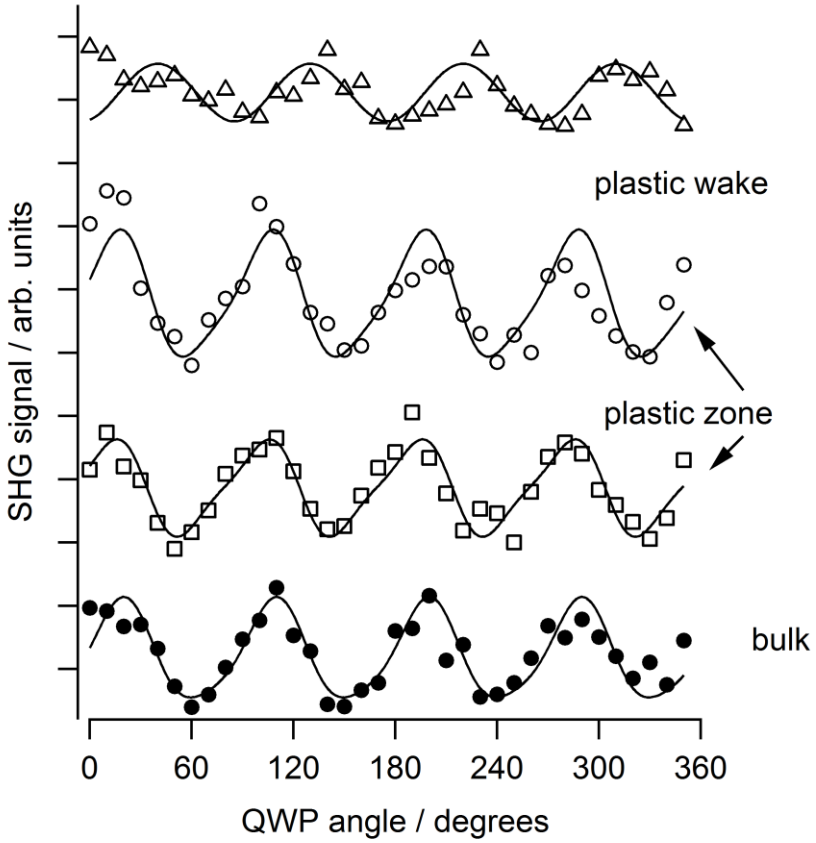

Figure 2. Polarization scans with initial p+s polarization state in four different spots on the surface. Data are offset for clarity and fitted to equation (4) (solid lines). The symbols correspond to the positions marked in Figure 1.

Figure 2 summarizes the data for four representative spots in different areas of the specimen, marked in Figure 1. Even prior to data fitting, Figure 2 demonstrates that the in-plane tensor component significantly differs between bulk and fatigued material. To avoid beam damage, each

data point was only averaged over 200 laser shots and noise arises mostly from shot-to-shot power fluctuations in the laser power (about 5%) and low signal intensities. For the measurement within the plastic wake, the mixed input polarization yielded noisy data, increasing fitting error. For this reason, $\chi^{(2)}_{zxx}$ values were obtained from a global fit to both p+s and p data sets. Additional data are shown in the supporting information. All initial fits yielded very low values for g_2 relative to f and were restrained to $g_2=0$ for the final fits. The results are summarized in Table 1. The data show that the in-plane component $g_1 \approx \chi^{(2)}_{zxx}$ is significantly enhanced within the plastic zone compared to bulk titanium and undergoes a 180° phase change in the plastic wake.

Table I. Fitted values of the expansion coefficients f and g for p-polarized second harmonic light. Error bars are determined from global fit errors to data with p+s and p incoming polarization states. The symbols correspond to the positions marked in Figure 1.

Position	**Symbol**	**f**	**g_1**	**g_1/f**
Bulk	●	1 ± 0.03	-0.14 ± 0.05	-0.14
Plastic zone	○	1.38 ± 0.08	-0.36 ± 0.11	-0.26
Plastic zone	□	1.05 ± 0.04	-0.43 ± 0.05	-0.41
Plastic wake	△	1.48 ± 0.09	1.04 ± 0.17	+0.71

The $\chi^{(2)}_{zxx}$ tensor component arises from lateral currents, which are related to the electronic density of states (DOS) as well as anisotropic stacking of lattice planes [38, 39]. A change of sign of $\chi^{(2)}_{zxx}$ was for example found by Güdde *et al.* for magnetic Ni and Co films of increasing thicknesses grown on copper surfaces [26]. They attributed this change to a 180° phase difference between the SH signals from copper s-electrons and Ni or Co d-electrons. A related phenomenon

was observed in a comparison of wavelength-dependent sum frequency spectra on Pt, Au and Ag surfaces, where the phase of the signal depends on whether s- or d-electrons are involved in the electronic transition [36].

The relative contributions of titanium s- or d-electrons to the second harmonic signal could be changed by dislocations, which alter the electronic density of states. Within the plastic zone, an increase in dislocations resulting from plastic deformation has been previously mapped by backscattered electron images [4]. The Ti DOS has also been found to depend on both structure and structural defects in density functional calculations [27, 28]. The close-packed hexagonal α phase at ambient temperature and pressure has a relatively low partial DOS from d-electrons at the Fermi level, while the bcc β phase found at higher temperatures and pressures possesses a much higher partial d-DOS[40]. Screw dislocations also introduce characteristic changes in the partial DOS of d-electrons, mostly within the occupied states about 0.5 eV below the Fermi level [28]. It is therefore conceivable that the changes in the sign and relative magnitude of $\chi^{(2)}_{zxx}$ are caused by a fatigue-induced alteration of the electronic density of states of the titanium specimen. The SHG signal currently derives from all transitions originating as far as 1.5 eV below E_F. The use of lower photon energy excitation for the SHG process compared to the current 1.5 eV could increase the sensitivity of the method to dislocations in titanium.

CONCLUSIONS

We have shown that the nonlinear optical response is different in the plastic zone ahead of a fatigue crack, where linear optical inspection shows no change in the material. In particular, we found that the magnitude of the $\chi^{(2)}_{zxx}$ tensor component, which is characteristic for lateral currents, is significantly enhanced within the plastic zone in comparison to bulk polycrystalline

titanium. A 180° phase change is found within the plastic wake which could be caused by an altered electronic DOS caused by dislocations.

There are several advantages to our nonlinear optical approach: it is possible to detect the response in a range of environments such as high pressure gases or liquids and with high time resolution for higher repetition rate laser systems; it is possible to detect a crack before it breaks through the surface, as long as the plastic zone around the crack tip extends to within a few nanometers from the surface; the spatial resolution is determined by the focal spot size of the laser beam used and is therefore adaptable to the grain size of the material under investigation. While the method is at present relatively time-consuming, we are currently developing a portable instrument based on a near-IR oscillator, which also circumvents the beam damage caused by amplified systems.

ACKNOWLEDGMENTS

This work was partly supported by an Engineering and Physical Science Council (EPSRC) Bridging the Gaps award. The authors would like to thank David Atkinson for electropolishing the titanium specimen. EP was in receipt of a Royal Society Wolfson Research Merit Award.

Supporting Information.

1. Full phase angle data from thermoelastic stress analysis
2. P-in, p-out line scans of SH intensity around the crack tip.
3. Polarization scans with incoming p+s and p polarizations.

AUTHOR INFORMATION

Corresponding Author

*E-mail: Heike.Arnolds@liverpool.ac.uk, ORCID Heike Arnolds: 0000-0002-5723-9309

Author Contributions

This manuscript is based on AK's final year project for a Masters in Engineering at the University of Liverpool in 2016. HA and EP conceived of the presented idea. HA and AK carried out and analyzed the SHG experiments, KS carried out and analyzed the TSA experiments. HA wrote the manuscript with contributions from all other authors. All authors have given approval to the final version of the manuscript.

Notes

During the write-up of this paper we became aware of related SHG research presented at the 253rd ACS meeting, San Francisco, 2017 [41].

REFERENCES

1. W. D. Callister, *Materials science and engineering : an introduction*, 7th ed. (John Wiley & Sons, New York, 2007).
2. E. Wolf, Engineering Fracture Mechanics **2** (1), 37-45 (1970).
3. A. Uguz and J. W. Martin, Materials Characterization **37** (2-3), 105-118 (1996).
4. Y. Yang, M. Crimp, R. A. Tomlinson and E. A. Patterson, Proceedings of the Royal Society A: Mathematical, Physical and Engineering Sciences **468** (2144), 2399-2415 (2012).
5. A. S. Patki and E. A. Patterson, Fatigue & Fracture of Engineering Materials & Structures **33** (12), 809-821 (2010).
6. O. M. Barabash, M. Santella, R. I. Barabash, G. E. Ice and J. Tischler, JOM **62** (12), 29-34 (2010).

7. N. Jia, R. L. Peng, G. C. Chai, S. Johansson and Y. D. Wang, Materials Science and Engineering a-Structural Materials Properties Microstructure and Processing **491** (1-2), 425-433 (2008).
8. N. Bloembergen, R. K. Chang, S. S. Jha and C. H. Lee, Physical Review **174** (3), 813-822 (1968).
9. K. B. Eisenthal, Chemical Reviews **106** (4), 1462-1477 (2006).
10. M. Fiebig, V. V. Pavlov and R. V. Pisarev, Journal of the Optical Society of America B-Optical Physics **22** (1), 96-118 (2005).
11. F. M. Geiger, in *Annual Review of Physical Chemistry* (2009), Vol. 60, pp. 61-83.
12. S. Roke and G. Gonella, in *Annual Review of Physical Chemistry, Vol 63*, edited by M. A. Johnson and T. J. Martinez (2012), Vol. 63, pp. 353-378.
13. Y. R. Shen, Nature **337** (6207), 519-525 (1989).
14. C. S. Tian and Y. R. Shen, Surface Science Reports **69** (2-3), 105-131 (2014).
15. G. Erley, R. Butz and W. Daum, Physical Review B **59** (4), 2915-2926 (1999).
16. I. L. Lyubchanskii, N. N. Dadoenkova, M. I. Lyubchanskii, T. Rasing, J. W. Jeong and S. C. Shin, Applied Physics Letters **76** (14), 1848-1850 (2000).
17. J. W. Jeong, S. C. Shin, I. L. Lyubchanskii and V. N. Varyukhin, Physical Review B **62** (20), 13455-13463 (2000).
18. A. Bonda, S. Uba and L. Uba, Applied Physics Letters **105** (19), 191608 (2014).
19. Y. Cho, F. Shafiei, B. S. Mendoza, M. Lei, T. Jiang, P. S. Ho and M. C. Downer, Applied Physics Letters **108** (15), 151602 (2016).
20. D. Ascienzo, S. Greenbaum, T. J. M. Bayer, C. A. Randall and Y. H. Ren, Acta Materialia **126**, 520-527 (2017).
21. P. C. Ray, Chemical Reviews **110** (9), 5332-5365 (2010).
22. N. K. Balla, C. Rendon-Barraza, L. M. Hoang, P. Karpinski, E. Bermudez-Urena and S. Brasselet, Acs Photonics **4** (2), 292-301 (2017).
23. F. X. Wang, F. J. Rodriguez, W. M. Albers, R. Ahorinta, J. E. Sipe and M. Kauranen, Physical Review B **80** (23), 233402 (2009).
24. A. Liebsch and W. L. Schaich, Physical Review B **40** (8), 5401-5410 (1989).
25. A. Liebsch, Applied Physics B **68** (3), 301-304 (1999).

26. J. Güdde, J. Hohlfeld and E. Matthias, Applied Physics B-Lasers and Optics **74** (7-8), 691-695 (2002).
27. N. Tarrat, M. Benoit, D. Caillard, L. Ventelon, N. Combe and J. Morillo, Modelling and Simulation in Materials Science and Engineering **22** (5), 055016 (2014).
28. E. Clouet, D. Caillard, N. Chaari, F. Onimus and D. Rodney, Nat Mater **14** (9), 931-936 (2015).
29. J. M. Vasco-Olmo, M. N. James, C. J. Christopher, E. A. Patterson and F. A. Díaz, Fatigue & Fracture of Engineering Materials & Structures **39** (8), 969-981 (2016).
30. F. Geiger, R. Stolle, G. Marowsky, M. Palenberg and B. U. Felderhof, Applied Physics B **61** (2), 135-141 (1995).
31. F. X. Wang, M. Siltanen and M. Kauranen, Physical Review B **76** (8), 085428 (2007).
32. C. Schriever, C. Bohley and R. B. Wehrspohn, Optics Letters **35** (3), 273-275 (2010).
33. C. Matranga and P. Guyot-Sionnest, The Journal of Chemical Physics **115** (20), 9503-9512 (2001).
34. B. Metzger, L. Gui and H. Giessen, Opt Lett **39** (18), 5293-5296 (2014).
35. F. Che, S. Grabtchak, W. M. Whelan, S. A. Ponomarenko and M. Cada, Results in Physics **7**, 593-595 (2017).
36. L. Dreesen, C. Humbert, M. Celebi, J. J. Lemaire, A. A. Mani, P. A. Thiry and A. Peremans, Applied Physics B **74** (7-8), 621-625 (2002).
37. J. Rudnick and E. A. Stern, Physical Review B **4** (12), 4274-4290 (1971).
38. A. V. Petukhov and A. Liebsch, Surface Science **320** (1-2), L51-L56 (1994).
39. H. Ishida, A. V. Petukhov and A. Liebsch, Surface Science **340** (1-2), 1-15 (1995).
40. M. Jafari, A. Jahandoost, M. Vaezzadeh and N. Zarifi, Condensed Matter Physics **14** (2), 23601 (2011).
41. A. Farnsworth, S. Averett, K. Rellaford, S. D. Smith and J. E. Patterson, presented at the 253rd ACS National Meeting, San Francisco, 2017 (unpublished).